Negative differential resistance in the Peierls insulating phases of TTF-TCNQ

Daiki Tonouchi,[1] Michio M. Matsushita,[1,*] and Kunio Awaga[1,2,†]

[1]*Department of Chemistry, Graduate School of Science, Nagoya University, Furo-cho, Chikusa-ku, Nagoya-City, Aichi 464-8602, Japan*

[2]*Research Center for Materials Science, Nagoya University, Furo-cho, Chikusa-ku, Nagoya-City, Aichi 464-8602, Japan*

(Received 22 May 2017; revised manuscript received 19 June 2017; published 14 July 2017)

Negative differential resistance (NDR) was observed in the most well known organic conductor, TTF-TCNQ, in its low-temperature Peierls insulator phase below 53 K. The voltage-current (V-I) characteristics below this temperature, measured by a four-probe method, exhibited unique NDR behavior, in which the $\mathrm{d}V/\mathrm{d}I$ versus conductivity (σ) plots had the inflection points at the three σ values without depending on temperature. These σ values were found to coincide with the conductivities at the three transition temperatures (53, 49, and 38 K) for the formation of the charge-density waves in TTF-TCNQ. This suggests that the electronic structure of the Peierls insulating phase of TTF-TCNQ is governed by the total carrier density, which is determined by not only thermal excitation but also carrier injection.

DOI: 10.1103/PhysRevB.96.045116

I. INTRODUCTION

TTF-TCNQ (tetrathiafulvalene-tetracyanoquinodimethane), the first "synthetic metal", has been investigated extensively since its synthesis in 1973 [1]. Recently, TTF-TCNQ has attracted new attention as a contact electrode material in organic electronics by virtue of its low-temperature sublimable property compared with metal electrodes [2]. The precise physical measurements for the Peierls state in TTF-TCNQ have already revealed the presence of internal transitions, namely, the formation of charge-density waves (CDWs) along the TCNQ and TTF chains at 53 and 49 K, respectively [3–5]. Below 49 K, there is a mismatch between the CDWs along the TCNQ and TTF chains in phase and periodicity (incommensurate phase). Below 38 K (the locking transition temperature), the periodicities of the two CDWs coincide with each other. In these low-temperature phases, higher-order nonlinear current-voltage (I-V) characteristics ($I \propto V^n$, $n \geqslant 2$) have been reported [6,7], caused by the sliding (depinning) of the CDWs under the applied electric fields. The order n of the nonlinear conductivity gradually increases with decreasing temperature, depending on the above temperature regions, and becomes negligible in the incommensurate phase between 38 and 49 K.

Negative differential resistance (NDR) is a typical nonlinear transport phenomenon in which the I-V profile shows a negative slope (differential resistance, $\mathrm{d}I/\mathrm{d}V$) in some regions. I-V profiles can be classified into N-and S-shaped NDR, in which the current decreases with increasing applied voltage [8] and the voltage decreases with increasing applied current [9], respectively. When voltage is plotted on the horizontal axis and the current is plotted on the vertical axis, they are classified as N-type and S-type NDR, respectively. S-type NDR has been reported on Mott insulator Cu-TCNQ thin film [10], TTF-CA with neutral-ionic transition [11], K-TCNQ with the spin-Peierls transition [12], and so on. NDR was also observed in the charge state of θ - $(BEDT\text{-}TTF)_2CsCo(SCN)_4$ [13] and in an ion-radical salt of a cyclophane-type donor, $CPTD{\cdot}Br{\cdot}(TCE)_2$ [14]. The former exhibited thyristor behavior [13], and the latter showed a relaxation of charge disproportionation upon current loading by x-ray crystal structure analysis [14]. Since NDR materials are expected to be applied to molecular memory devices [15] and inverters [16], they are attracting new research interest in the field of molecular conductors. In the present paper, we report the discovery of NDR in TTF-TCNQ in the low-temperature Peierls phase. NDR behavior is found to critically depend on the temperature ranges separated by the three transition temperatures, 53, 49, and 38 K, consistent with the reported higher-order nonlinear I-V characteristics ($I \propto V^n, n \geqslant 2$). In contrast, it is also found that the inflection points in the V-I characteristics in the whole temperature range below 53 K can be well normalized by the sample conductivity.

II. EXPERIMENT

A single TTF-TCNQ crystal was grown by the liquid-phase reaction processes of TTF and TCNQ through diffusion in acetonitrile solution at room temperature (ca. 290 K). A typical size of the crystal was about $2 \times 0.2 \times 0.05\,\mathrm{mm}^3$. For four-probe conductivity measurements, four gold wires with a diameter of 25 μm were attached to the crystal by gold paste along the long axis of the crystal corresponding to the b axis (parallel to the π-staking direction). The outer two electrodes for current application were attached around the crystal to apply a uniform current density through the whole crystal cross section, because the conductivity of TTF-TCNQ has relatively large anisotropy along the crystal axes. A typical sample picture is shown in Fig. S1 in the Supplemental Material (SM) [17]. The sample was then connected and mounted to a sample probe and placed in a cryostat (Quantum Design, PPMS). The transport properties were investigated in the four-probe current-applying voltage measurement (V-I) method and the voltage-applying current measurement (I-V) method by an ADVANTEST R6245 source meter in direct current mode and pulse mode controlled by a PC through the GP-IB interface with custom-made software.

Since crystal often breaks through the conductivity measurements, especially at the temperature sweeping, data were taken on three crystals in this study. Since the observed values,

*mmmatsushita@nagoya-u.jp

†awaga@mbox.chem.nagoya-u.ac.jp

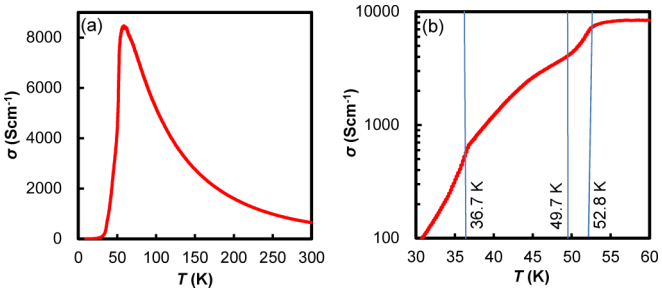

FIG. 1. Temperature dependence of conductivity of TTF-TCNQ in the whole measured temperature range (a) and below the Peierls transition temperature (b).

such as current (I) and voltage (V), are different for the different samples due to the difference in the sample size, the values are normalized to a relative values or converted to size-independent values, such as current density J ($\mathrm{A\,cm^{-2}}$), electric field E ($\mathrm{V\,cm^{-1}}$), and conductivity σ ($\mathrm{S\,cm^{-1}}$). Even so, there should be some experimental errors due to the errors at size measurement of small crystals. The relation between the samples and the data are summarized in the Supplemental Material (SM) [17].

III. RESULTS

A. Temperature dependence of the conductivity of TTF-TCNQ

The temperature dependence of the conductivity of the single TTF-TCNQ crystal was measured upon cooling in the temperature range from 300 to 2 K at a sweep rate of 1 K/min, by loading a constant current of 1 mA ($20.8\,\mathrm{A\,cm^{-2}}$). The results are shown in Fig. 1(a), in which the metallic conducting behavior above 59 K and sharp drop-down of conductivity below 53 K due to the Peierls transition at this temperature are clearly seen. The low-temperature behavior is shown in Fig. 1(b) on an enlarged scale. One can clearly see three inflection points caused by the presence of the three CDW phases after the Peierls transition. These results are consistent with the past reports [3].

B. V-I measurement in low-temperature phase

The four-probe current-sweeping voltage measurement (V-I) was carried out at 20, 30, 40, 50, and 60 K [Fig. 2(a)]. In contrast to the monotonous increase in the V-I characteristics

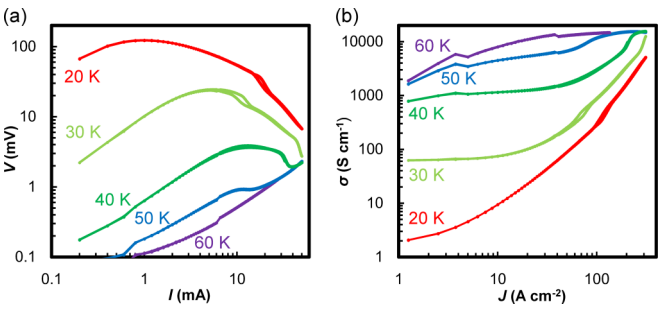

FIG. 2. V-I characteristics of TTF-TCNQ at various temperatures (a), and σ-J characteristics derived from the V-I data (b).

at 60 K, namely, above the Peierls transition temperature (53 K), the V-I curves exhibit nonlinear behavior below this temperature. At 50 K, an NDR region appears, and it grows as the temperature decreases. Figure 2(b) shows the relation between the sample conductivity σ and the current density J (σ-J characteristics) derived from the V-I data. At all the measured temperatures shown here, conductivity increases monotonously as increasing current density despite the appearance of NDR.

Figures 3(a)–3(f) show the temperature dependence of the electric field versus applied current density (E-J) profiles, derived from the V-I curves, in the respective ranges (54–48 K, 46–40 K, 38–32 K, 30–22 K, 20–12 K, and 10–4 K). In the higher-temperature range [Fig. 3(a)], the E-J curve can be separated into two regions: a nonlinear transport region at low loading current density and a linear transport region at high current densities. When the data are plotted in a J-E graph, we can see an S-shaped relationship (Fig. S2(a) in the SM [17]). Below 46 K, E-J plots varied from the simple S shape to having some complex structures as shown in Figs. 3(b)–3(d). Hystereses are observed in the E-J plots below 44 K and become clearer below 34 K, and the hysteresis region moved to higher current values with decreasing temperature. In addition, clear inflection points appear in the NDR regions below 36 K [Fig. 3(c)]. In the further low-temperature region as shown in Figs. 3(e) and 3(f), the peak (highest value) of the electric field increases rapidly with decreasing temperature whereas the threshold current density (current density at the highest electric field) becomes lower monotonously (also seen in Fig. S3(c) [17]). As the result, NDR is observed in most of the measured current density range in Figs. 3(e) and 3(f). However, the change becomes smaller at the lowest-temperature range and the E-J curves for 4 and 6 K are very close to each other as shown in Fig. 3(f). The fact that the transport property becomes temperature insensitive in this temperature range would be explained in terms of the Joule heating by the applied electric power.

To clarify the origin of the hysteresis, we also performed the V-I measurements by using a pulse current at 30, 32, 34, 36, and 38 K. The results are shown in Fig. 4 (solid curves), together with the data obtained by a continuous sweep method on the same sample (broken curves) [18]. The results of the pulse current measurements do not have hysteretic behavior and the curves agree with those in the forward (current increasing) scan of the continuous sweep method. Hysteretic behavior has been reported in relation to the temperature dependence of TTF-TCNQ conductivity around the locking transition at 38 K [19,20], suggesting that the V-I measurement in this region causes the similar phase transition. On the other hand, as indicated by the straight line in Fig. 4, the electric fields at the inflection points on the E-J plots below 38 K are proportional to the loaded current densities. This means that the inflection points are strongly related to the sample conductivity, $\sigma = 1/\rho = J/E$. To clarify this relationship, several parameters were compared with the sample conductivity as shown in Fig. S4 [17]. Among them, the relationship is clearly seen in the plots of the differential resistance ($\mathrm{d}V/\mathrm{d}I$) against the conductivity σ as shown in Fig. 5. In the $\mathrm{d}V/\mathrm{d}I$-σ plots, the inflection points appear at the same conductivity. Furthermore, the specific conductivities, 750, 3800, and 7500 $\mathrm{S\,cm^{-1}}$,

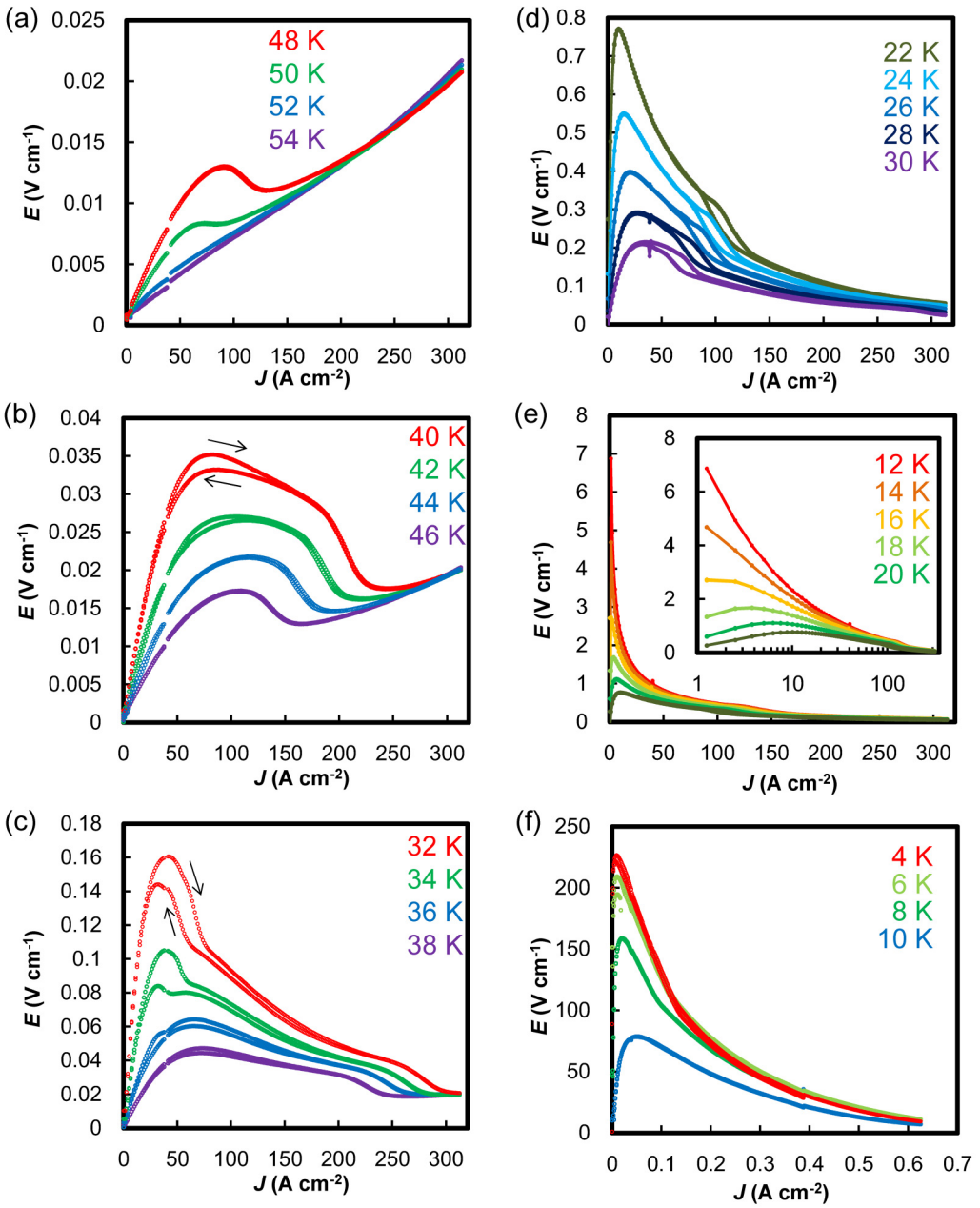

FIG. 3. E-J plots of TTF-TCNQ at various temperatures (a) 54–48 K, (b) 46–40 K, (c) 38–32 K, (d) 30–22 K, (e) 20–12 K; the inset shows the logarithmic horizontal scale, (f) 10–4 K.

also agree with the conductivities of the three transition temperatures, 38, 49, and 53 K, respectively. On the other hand, excluding around the inflection point, the dV/dI value decreases monotonously with increasing σ although there are differences in the absolute values by the temperature. The negative dV/dI value means the appearance of NDR. These suggest that the electronic state in the low-temperature phase of TTF-TCNQ below 53 K could be well described as the function of the system conductivity itself. The effect of the applied current density is also observed in the temperature dependence of the conductivity of TTF-TCNQ, as shown in Fig. 6. The larger the applied current density, the larger the conductivity. However, the sample conductivity is not simply proportional to the applied current density at these temperatures. The conductivities at 0.1 and 1 mA are nearly the same above 40 K, but they bifurcate at 38 K, which is the locking temperature of the CDWs along the TTF and TCNQ chains. The conductivities at 1 and 5 mA bifurcate at 53 K, which corresponds to the formation of a CDW along the TCNQ chain. In cases where the applied currents are larger than 5 mA, the conductivity increases across the whole temperature range up to 60 K in the metallic phase. These results suggest that the capable current value with the corresponding transport mechanism for each temperature region is limited, and that the excess current value causes the excitation of the upper conducting mechanism in a stepwise manner.

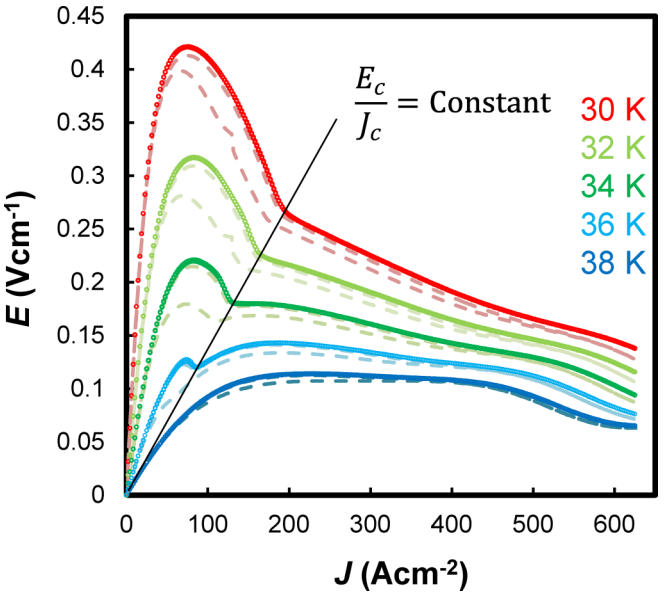

FIG. 4. *E*-*J* characteristics by pulse measurement (solid line, period: 1 s; pulse width: 100 ms; integration time: 1 ms) and by continuous current sweep measurement (dashed line).

IV. DISCUSSION

A. Transport measurement methods

Whereas NDR behavior is classified as N or S type, as described in the Introduction, the NDRs observed in bulk crystals of organic conductors are always the latter. In the case of S-type NDR, with an increase in the current the sample resistance decreases greatly, more than the current's rate of increase. In most cases reported so far, the *I*-*V* characteristics are measured in a situation in which a load resistor is inserted in series to limit the largest current, and the voltage drop at the load resistor is subtracted to plot the *I*-*V* for the sample. However, in this case, neither the voltage nor the current applied to the sample can be controlled precisely. Since up to three current values can be taken with the same voltage in the S-type NDR (as shown in Fig. S2(a) in the SM [17]), voltage oscillation between the states may take place in some cases. In fact, some investigations were carried out to stabilize the oscillation of an S-type NDR system by controlling the time constant, which depends on the additional resistors and capacitors [21–23]. On the other hand, when a voltage was applied to a sample showing S-type NDR without a load resistor, the current monotonically increased as the voltage increased and only the rapid increase of the current should be observed [24–26] without a negative slope. This should be the reason why NDR has not been observed in TTF-TCNQ so far. Since the sample resistance in the S-type NDR system decreases monotonously with increasing current density as shown in Fig. 2(b), the current-applying voltage measurement method (*V*-*I*) is preferable to figure out the transport behavior in this system. Furthermore, when the sample has a semiconducting nature, the interface with the metal electrode may have nonlinear conductivity due to the formation of a Schottky barrier in some cases. For these reasons, a dc four-terminal method was applied, in which four

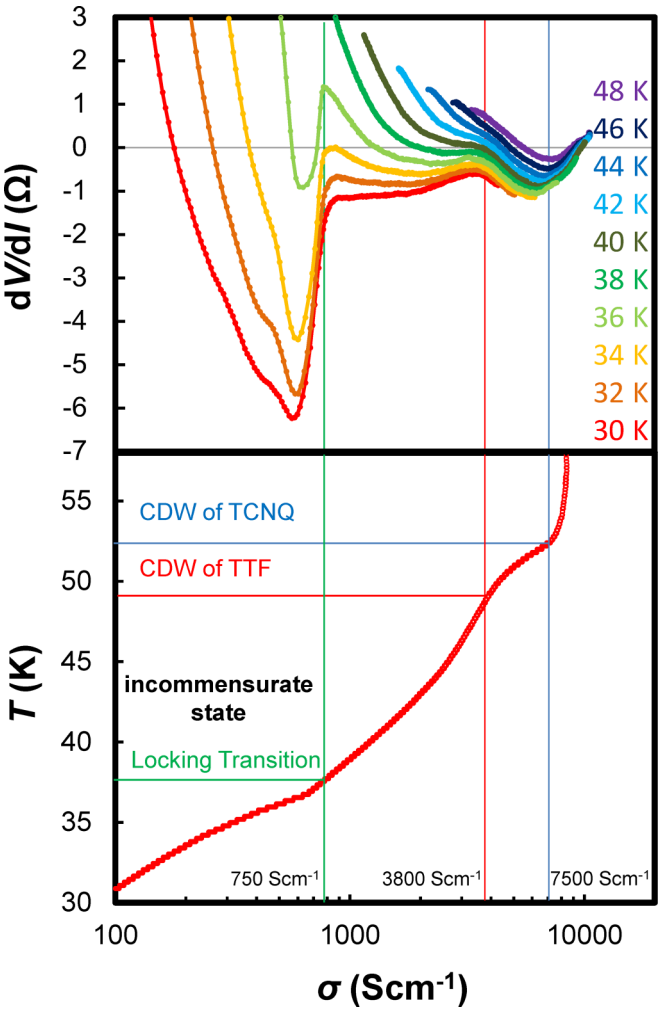

FIG. 5. Relationship between the dV/dI versus sample conductivity σ derived from the *V*-*I* characteristics accompanied by the temperature dependence of the conductivity.

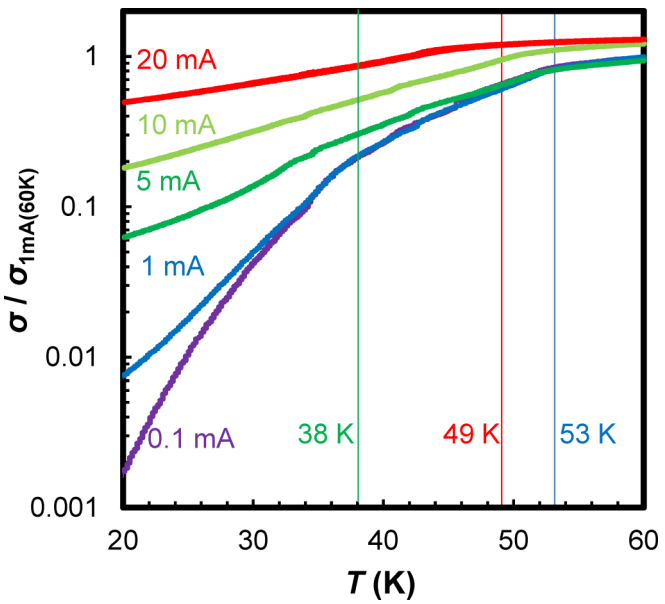

FIG. 6. Temperature dependence of the conductivity of TTF-TCNQ crystal with several different current values.

electrodes were attached to the sample and the voltage on the sample was measured with the different pairs of electrodes from current application. Actually, reproducible results were stably obtained repeatedly with respect to the behavior of NDR when the current sweep was performed by the direct current four-terminal method.

On the other hand, higher-order I-V ($I \propto V^n$, $n \geqslant 2$) and NDR behavior are often doubted as effects of the Joule heat because the resistance of the semiconducting sample decreases through thermal excitation. Generally, conductors with an insulating ground state exhibit thermally activated conductivity, and thus it is possible to show nonlinear I-V characteristics through the Joule heat. However, when the thermal effect of the Joule heat was taken into account in this study from the thermal flow through four gold wires (25 μm ϕ and 3 mm long at maximum) with the thermal conductivity of gold (420 $\mathrm{W\,m^{-1}\,K^{-1}}$), the temperature difference of the sample from the system temperature was estimated to be ca. 2 K at maximum with a maximum consumed power of 600 μW as shown in Fig. S4(d) in the SM [17]. In this case, the conductivity of the sample at 30 K corresponds to that at 49 K under loading current, and this value cannot be explained from the thermal effect of the Joule heat (2 K in maximum). In addition, to minimize the effect of Joule heat further, measurements were also carried out instantaneously by applying pulse current in addition to the usual continuous current sweep method. The fact that the V-I characteristics obtained by the continuous sweep method and the pulse method well agreed with each other also suggests the small effect of the Joule heat. Therefore, the effect of the Joule heating would not be the main reason for NDR above 30 K, mainly discussed in this study, whereas it would take an important place in the lowest-temperature range (around 4 K) as described in the Results section.

B. Origin of NDR and temperature dependence in TTF-TCNQ

In general, S-type NDR is caused by some excitation mechanism from an insulating ground state to a higher-conductivity excited state by current application. At that time, when the rate of increase in conductivity is greater than the rate of change of the current, the voltage drop has a negative slope relative to the current and can be observed as NDR. Regarding the organic conductors exhibiting NDR so far reported, they often have CDW states, such as charge disproportionation and charge ordering, and the melting of the high- resistivity CDW state to a higher-conductivity state is caused by the applied current, although the mechanisms underlying this phenomenon have not been clarified in some cases.

In the case of TTF-TCNQ, while it shows metallic conducting behavior due to the uniform π-staking structure in the high-temperature phase, it turned out to be insulating in the low-temperature phase below 53 K by seven orders of magnitude, down to 4.2 K, accompanied by lattice distortion in the π-staking column based on the Peierls transition. Therefore, inversely, the melting of the distorted structure in the low-temperature phases to the uniform structure by the application of current could be a cause of NDR, although there is no direct evidence of structural change during the appearance of NDR in this stage. However, although NDR has not been reported in TTF-TCNQ, higher-order I-V characteristics ($I \propto V^n$, $n \geqslant 2$) have been reported in detail and the underlying mechanism has been discussed [24–26]: The threshold voltage dependence on the three Peierls insulator phases is explained in terms of the depinning and sliding of the CDW. Below 53 K, the periodicity of CDW on the TCNQ chain coincides with the periodic distortion of the TCNQ chain caused by the CDW itself and the charge propagation (current) is pinned by the interaction through the band-gap formation at $2k_\mathrm{F}$ in the band dispersion diagram (Peierls transition). Below 49 K, the same phenomenon takes place on the TTF chain ($4k_\mathrm{F}$). Although the periodicities of CDWs along TTF and TCNQ chains are incommensurate with each other below 49 K, they become integer ratio and the CDWs are immobilized more strongly below 38 K (interlocking). By applying a strong electric field (threshold electric field, E_T) to overcome the pining potential energy, the sliding motion of CDW (charge propagation) is quickly recovered, and the higher-order I-V curve ($I \propto V^n$, $n \geqslant 2$) is observed [6,7]. Although the expression is different due to the difference in the measurement method (I-V and V-I), the origin of the reported higher-order I-V and that of the NDR in this study should be basically the same. As described above, the insulating states of TTF-TCNQ under the Peierls transition temperature are explained in terms of the pinning of the sliding motion of the CDW by the periodic distortion potential of the lattice caused by the CDW itself, and by the interaction with the CDW of the other chains of opposite charge (TTF and TCNQ). Since the flowing current below the Peierls transition temperature is explained as the sliding of the CDW, a certain point on the lattice will feel the periodic change (oscillation) of the electric potential from the sliding CDW. If the lattice distortion cannot follow the periodic change of the electric potential caused by the sliding of CDW, the amplitude of the distortion will be weakened by increasing current density because the higher current density means the faster sliding motion of the CDW (i.e., faster oscillation). A similar mechanism could be also discussed on the interaction between the CDWs of the opposite charges. Therefore, there should be positive feedback mechanisms to increase the conductivity by applying current density to express NDR through the weakening of the pinning potential of CDW.

The other new finding, that the conducting behavior of TTF-TCNQ below 53 K seems to depend on the conductivity of the system itself as shown in Fig. 5, needs further discussion. It was found that the inflection points in the E-J curves for different temperatures were well sorted in terms of the conductivity of the sample. Usually, the conductivity of the material is considered as the result of the electronic structure of the sample and the function of the environmental variables, such as temperature and pressure. Therefore, the relationship seems opposite in the current case. In the case of TTF-TCNQ, each phase under 53 K shows S-type NDR. As described above, S-type NDR is explained as the phenomenon that the sample conductivity increases as the current increases. In other words, the conductivity of the NDR system could be changed by the applied current (two orders of magnitude, in this study). Since the conductivity σ is expressed as the product of the carrier density n, elemental charge e, and mobility μ, and since e and μ are supposed to be constant in the same crystal phase,

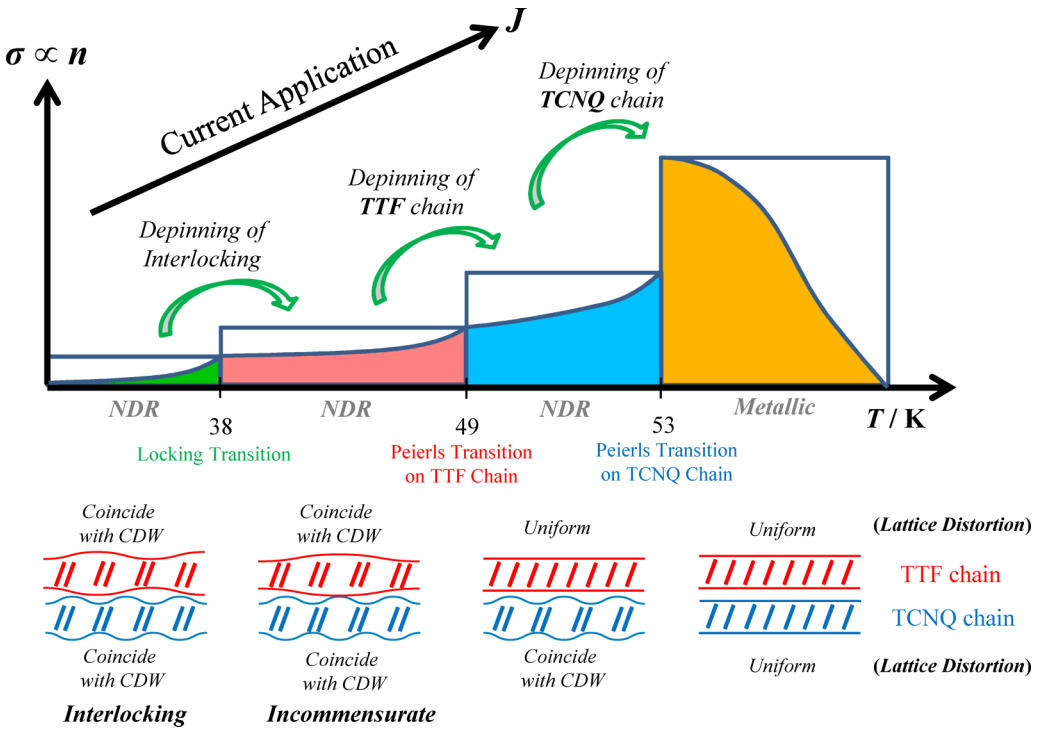

FIG. 7. Schematic drawing of the plausible mechanism for the conductivity change upon current application in TTF-TCNQ.

the conductivity of the sample could be mainly expressed as the function of n. Namely, n is not only excited thermally, but also induced by externally applied current in the NDR system. Therefore, the observed conductivity dependence would originate from the dependence on the carrier density n. However, the carrier density n should have some upper limit for each carrier transport mechanism even in the NDR system. Actually, the slope of the E-J curves in typical NDR systems turned out to be positive again in the higher current density region. This situation is also seen in TTF-TCNQ just below 53 K as shown in Fig. 3(a). However, if the system has a higher conductive phase, the phase transition will take place to have higher carrier density n by increasing current density further. In the case of TTF-TCNQ, two and three upper conducting phases with higher conductivities exist in the phases below 49 and 38 K, respectively. In fact, the E-J curves of TTF-TCNQ have complex structures in the lower-temperature region, and the structures were well characterized in relation with the three phase transitions at 53, 49, and 38 K. This phenomenon could be explained in terms of the phase transition to the higher conducting state, caused by the induced carrier. In TTF-TCNQ, although the band gap is formed and insulated through the Peierls transition below 53 K, the insulating electronic structure is caused by the system's electrons themselves and the electric current is nothing but moving electrons (or holes) in the sample itself. Therefore, the NDR and phase transition through V-I measurements could be attributed to the function of carrier density in the insulating states of TTF-TCNQ below the Peierls transition temperature as drawn in Fig. 7.

V. CONCLUSION

Negative differential resistance (NDR) was found and added as a new feature of TTF-TCNQ, the most well known and well investigated organic conductor. NDR was observed in the whole measured temperature range below 53 K, which corresponds to the Peierls transition temperature, whereas the structures in E-J curves including NDR depend on the three phases below 53, 49, and 38 K. Although the origin of NDR would be the same as that of the reported higher-order I-V characteristics ($I \propto V^n$, $n \geqslant 2$), it was revealed that both NDR in V-I characteristics measurements and the phase transitions in the temperature dependence measurements could be explained as functions of the charge carrier density in the sample because the three inflection points observed in both plots had the same conductivity. This feature originated from the characteristic electronic structure of TTF-TCNQ. Since the Peierls phase transition depends mainly on the strong correlations among electrons in the quasi-one-dimensional electronic structure, the electronic state would be quite sensitive for the charge carrier density regardless of the origin of the carrier, whether it is thermally excited or externally induced by the current application.

ACKNOWLEDGMENT

This work was supported by JSPS KAKENHI Grant No. JP16H00962.

[1] J. Ferraris, D. O. Cowan, V. V. Walatka, and J. H. Perlstein, J. Am. Chem. Soc. **95**, 948 (1973).

[2] B. Mukherjee and M. Mukherjee, Langmuir **27**, 11246 (2011).

[3] C. K. Chiang, M. J. Cohen, P. R. Newman, and A. J. Heeger, Phys. Rev. B **16**, 5163 (1977).
[4] Y. Tomkiewicz, R. A. Craven, T. D. Schultz, E. M. Engler, and A. R. Taranko, Phys. Rev. B **15**, 3643 (1977).
[5] K. Saito, Y. Yamamura, H. Akutsu, M. Takeda, H. Asaoka, H. Nishikawa, I. Ikemoto, and M. Sorai, J. Phys. Soc. Jpn. **68**, 1277 (1999).
[6] M. J. Cohen, P. R. Newman, and A. J. Heeger, Phys. Rev. Lett. **37**, 1500 (1976).
[7] M. J. Cohen and A. J. Heeger, Phys. Rev. B **16**, 688 (1977).
[8] L. Liu and W. Leung, Phys. Rev. Lett. **33**, 1145 (1975).
[9] Z. Ji, C. Yang, K. Liu, and Z. Ye, J. Cryst. Growth **253**, 239 (2003).
[10] R. S. Potember, T. O. Poehler, and D. O. Cowan, Appl. Phys. Lett. **34**, 405 (1979).
[11] Y. Tokura, H. Okamoto, T. Koda, T. Mitani, and G. Saito, Phys. Rev. B **38**, 2215 (1988).
[12] R. Kumai, Y. Okimoto, and Y. Tokura, Science **284**, 1645 (1999).
[13] F. Sawano, I. Terasaki, H. Mori, T. Mori, M. Watanabe, N. Ikeda, Y. Nogami, and Y. Noda, Nature **437**, 522 (2005).
[14] M. M. Matsushita and T. Sugawara, J. Am. Chem. Soc. **127**, 12450 (2005).
[15] S. Shin and K. R. Kim, Jpn. J. Appl. Phys. **54**, 06FG07 (2015).
[16] J. Shim, S. Oh, D. Kang, S. Jo, M. H. Ali, W. Choi, K. Heo, J. Jeon, S. Lee, M. Kim, Y. J. Song, and J. Park, Nat. Commun. **7**, 13413 (2016).
[17] See Supplemental Material at http://link.aps.org/supplemental/10.1103/PhysRevB.96.045116 for additional information on the used samples and data on the conducting properties of TTF-TCNQ, such as J-E, I-σ, V-σ, $\mathrm{d}V/\mathrm{d}I$-σ, P-σ, and $\mathrm{d}V/\mathrm{d}I$-I curves, derived from V-I measurements with brief descriptions.
[18] Although the shape of the E-J curves for the same temperature in Figs. 3 and 4 are almost identical to each other, J and E at the characteristic peaks in the both figures had different values, because the data for these figures are taken on different crystals as described in the SM [17]. However, J and E for the same material should be basically the same even with the different crystals because these values are normalized by length and cross-sectional area, respectively, to be size-independent parameters. The observed differences in Figs. 3 and 4 might be due to the experimental error in the size when measuring small crystals.
[19] J. R. Cooper, J. Lukatela, M. Miljak, J. M. Fabre, L. Giral, and E. Aharon-Shalom, Solid State Commun. **25**, 949 (1978).
[20] S. Kagoshima, T. Ishiguro, and H. Anzai, J. Phys. Soc. Jpn. **41**, 2061 (1976).
[21] H. Kishida, T. Ito, A. Ito, and A. Nakamura, Appl. Phys. Exp. **4**, 031601 (2011).
[22] K. Awaga, K. Nomura, H. Kishida, W. Fujita, H. Yoshikawa, M. M. Matsushita, L. Hu, Y. Shuku, and R. Suizu, Bull. Chem. Soc. Jpn. **87**, 234 (2014).
[23] K. Okamoto, T. Tanaka, W. Fujita, K. Awaga, and T. Inabe, Phys. Rev. B **76**, 075328 (2007).
[24] R. C. Lacoe, H. J. Schulz, D. Jerome, K. Bechgaard, and I. Johannsen, Phys. Rev. Lett. **55**, 2351 (1985).
[25] R. C. Lacoe, J. R. Cooper, D. Jerome, F. Creuzet, K. Bechgaard, and I. Johannsen, Phys. Rev. Lett. **58**, 262 (1987).
[26] W. Wonneberger and F. Gleisberg, Solid State Commun. **23**, 665 (1977).